Article

Significance of Sonic Velocities in Limestones and Dolostones: A Comprehensive Study Revealing Limited Impact of Mineralogy

Ralf J. Weger [1,*], Gregor T. Baechle [2], Shouwen Shen [3] and Gregor P. Eberli [1]

1 Department of Marine Geosciences Rosenstiel School of Marine, Atmospheric, and Earth Science, University of Miami, 4600 Rickenbacker Causeway, Miami, FL 33149, USA
2 Benerco LLC, Katy, TX 77494, USA
3 Aramco, Dhahran 31311, Saudi Arabia
* Correspondence: rweger@miami.edu; Tel.: +1-305-421-4834

Abstract: Seismic reflection data and implicitly sonic velocity are undoubtedly the most important source of information for large-scale subsurface characterization. Yet, deriving reservoir and fluid flow properties from acoustic data is still challenging in carbonates, which display large acoustic velocity variations that contest many of the conventional assumptions regarding wave propagation in porous media. In this comprehensive study on 370 carbonate samples (247 limestones and 123 dolomites), we re-evaluate the impact of mineral velocity on bulk rock acoustic properties of dolomite and limestone by assessing the link between sonic velocity and the rock's pore geometry. We quantify pore size and pore network complexity using parameters from both digital image analysis (DIA) and the extended Biot theory (EBT). We then compare DIA and EBT parameters to assess the impact of pore network geometry versus mineral velocity on the acoustic velocity of carbonate rocks. We explore the usefulness of EBT parameter γ_k in improving permeability estimates. Published values of velocity indicate that dolomites exhibit higher velocities than limestones at any given porosity. Our laboratory measurements of acoustic velocity, however, reveal that both dolomites and limestones show extreme variations in sonic velocities where samples with compressional velocity of ~5000 m/s may range in porosity from 5% to 25% and samples with porosity of ~20% may range in velocity from ~4000 m/s to 5700 m/s. Through the quantitative assessment of the pore network in our samples we document that pore network geometry has much more impact on the acoustic velocity of carbonates than variations in mineralogy, in this case dolomite and calcite. Most of the dolostone samples studied are dominated by small pores, resulting in relatively low velocities for their given porosity, while limestones with similar velocity–porosity values often possess simpler pore networks with larger pores. This pore size difference offsets the faster velocity of dolomite. The extended Biot theory parameter γ_k, captures this variation in pore size and internal geometry and exhibits a strong correlation to specific surface. Moreover, γ_k captures the impact of internal pore geometry on acoustic velocity, providing the basis for challenging existing assumptions regarding the importance of mineral velocity. By quantifying internal geometry, γ_k can improve permeability estimates in reservoir characterization and enhance evaluations of producibility and injectability. With that, it has direct implications on general geophysics, hydrocarbon exploration, and CCS initiatives.

Keywords: acoustic velocity; permeability; carbonate rocks; dolomite; carbon capture storage; rock microstructures; petrophysical properties

1. Introduction

Given that carbonate rocks account for more than 50% of the world's proven hydrocarbon reserves [1] it is not surprising that their physical properties have been important for oil and gas exploration for decades. Seismic data are the most dominant source of subsurface information for reservoir characterization and acoustic velocity, implicitly, is one of the most influential attributes allowing geoscientists and engineers to interpret

the structure and properties of subsurface formations. In recent years, in the context of carbon capture and storage, even depleted, sealed carbonate reservoirs have gained again in importance. Carbonate rocks often show velocity–porosity relationships that are much less predictable than those in siliciclastic rocks because of complex and heterogeneous pore systems [2–4]. Rafavich, Kendall [5] presented data supporting their claim that bulk density and mineralogy influence acoustic velocity, while variations in pore type have only negligible effects. Nonetheless, the impact of diverse internal pore geometries on acoustic velocity of carbonates has been a subject of discourse for decades [2,6–19]. Most of these investigations provide evidence that alterations in pore configurations and the overall pore network structure, whether at a macroscopic or microscopic level, constitute the primary factors in the weak correlations observed between porosity and velocity in carbonate formations.

The complex pore systems of carbonate rocks also make it difficult to predict permeability from porosity in carbonate rocks [20]. In carbonates, both velocity–porosity and porosity–permeability relationships are difficult to predict without information regarding microtexture types and/or particle morphology [21–23]. Consequently, the determination of porosity from velocity, for example, when performing seismic inversion and the estimation of permeability from porosity in carbonate formations, contains large uncertainties, even in cases where the mineralogy (dolomite versus calcite) is well-established.

Digitized values from dolomite and limestone samples from the "typical rock property data" appendix of Mavko, Mukerji [24] result in distinct correlations in a velocity–porosity plot (Figure 1). An F-test on the hypothesis that correlation coefficients for slope and intersection of velocity vs. porosity show evidence of an interaction effect returned a value of F = 7.85, *p* = 0.0057, indicating that the two populations are in fact different. However, the rather large difference between the dolostone and the limestone intercept suggests that in addition to matrix mineral differences other factors might be in part responsible.
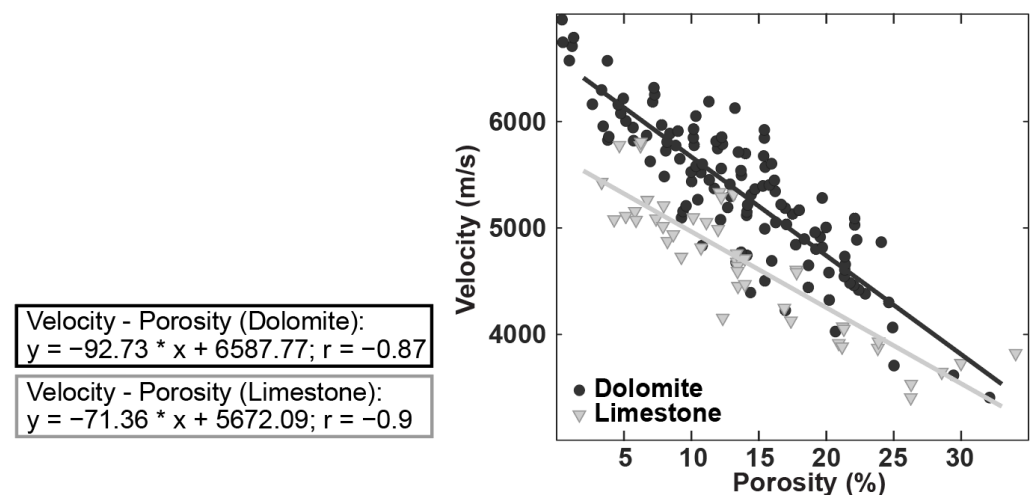
Figure 1. Compressional velocity vs. porosity of samples from Mavko and Mukerji [25] showing different correlations for dolostones and limestones.

Most basic properties of the different carbonate minerals (dolomite, aragonite, and calcite), and their differences, have been studied extensively [24]. Single-crystal calcite velocities have been determined by Dandekar [26] using the pulse-echo method. His results agreed with measurements published even earlier, but there are only very few documented examples [27–29]. Single-crystal dolomite velocities are even less frequently found, and none are easily accessible. Gebrande [30] shows substantially higher velocities for single-crystal dolomite than those published for single-crystal calcite. It is a generally accepted fact that, in the absence of pore geometry variations, dolomite has higher density and acoustic velocity than calcite. Although one might imagine that the acoustic behavior of rocks composed almost entirely of calcite, aragonite, and dolomite would be quite

simple [6], the impact of minerology variation on the acoustic velocity of carbonate rocks as compared to the impact of variations in internal geometry remains unclear and more importantly unquantified.

Fabricius, Baechle [31] enhanced permeability estimation in carbonates by relating detrended VpVs ratio to specific surface as defined by Kozeny [32]. Based on the assumption that a link exists between VpVs ratio and the rock's internal geometry as described by specific surface, their main conclusion was that both VpVs ratio and permeability are dependent on porosity and the specific surface of the rock. Moreover, the relationship is not controlled by depositional texture or carbonate mineralogy.

Weger, Eberli [33] documented how extended Biot theory parameters (f_k and γ_k) derived from acoustical measurements of limestones relate to digital image parameters derived from full thin sections cut directly from the core plugs used for velocity measurements. This analysis establishes a clear relationship between EBT frame flexibility and the internal pore geometry of limestones that enables the quantification of limestone pore characteristics from acoustic data. This correlation underscores the potential for significantly enhancing permeability estimates solely from acoustic velocity data. It implies that by performing joint inversion for γ_k and porosity rather than porosity alone, permeability estimation could be achieved using seismic data.

In this study, we document the impact of mineral composition and the impact of internal geometry on acoustic velocity of carbonate rocks. We use pore structure quantifications obtained directly from thin sections as described in [9] and we quantify internal pore geometry using the topological parameters f_k and γ_k directly derived from acoustic velocity using the extended Biot theory (EBT) [33,34]. This analysis allows us to document how the influence of microstructure is much stronger than that of mineralogy (in the case of dolomite vs. calcite). In addition, this study shows how this influence can be quantified using acoustic data by applying the extended Biot theory. This quantification of the pore structure allows improvement in the permeability predictions from acoustic data regardless of mineralogy, a benefit regular Biot theory is not capable of providing.

2. Dataset

For this study, we compiled a comprehensive dataset of 370 carbonate core plugs, 247 limestones and 123 dolostones, from studies performed within the CSL—Center for Carbonate Research. To ensure representativeness we selected eight different locations and four different geologic time periods (see Tables 1 and 2). From the Neogene we used 58 samples from a carbonate buildup in Turkey, 25 samples from the Marion Plateau (ODP Leg 194), and 35 samples from the Maldives (IODP Leg 359). Older samples from the Cretaceous Period are from two different Middle Eastern formations (78 and 38, respectively) and 38 samples from the Maiella Mountains in Italy. In addition, we used 59 samples from a Permian formation in the Middle East and 39 samples from the Mississippian Madison Formation (Figure 2). Core plugs from several different intervals in the above-listed formations provide a comprehensive range of porosity and various rock and pore types throughout the datasets. Thin sections corresponding to each plug sample were used for digital image analysis. All samples are predominantly composed of carbonates (calcite or dolomite) and contain only minor amounts of insoluble materials (~1–2%). All samples were classified according to Dunham [35] and contain examples of grainstone, packstone, rudstone, wackestone, floatstone, and mudstone. In addition, all samples were classified according to Choquette and Pray [36], illustrating the diversity of pore types including micromoldic, intraparticle, intercrystalline, interparticle, moldic, and vuggy pores.
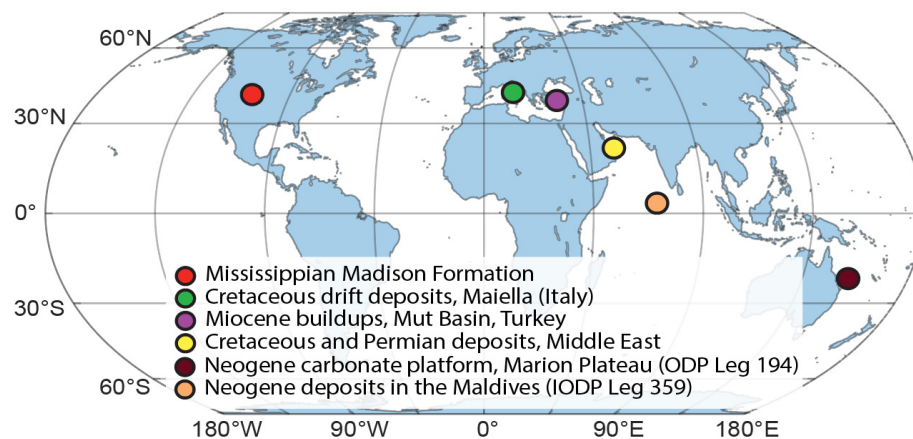
Figure 2. Map showing the locations of samples used in this study. In red, dolostone samples from the Madison Formation in Montana; in green, limestones from the Orfento Formation in Italy; in purple, shallow marine deposits from southern Turkey; in yellow, both dolostones and limestones from the Middle East; and in orange and brown, carbonate drift deposits from the Kardiva Channel in the Maldives and the Marion contourite drift system offshore eastern Australia.

3. Methods

3.1. Petrophysical Measurements

Porosity was determined from the difference between the volume calculated from the dimensions of the core plug and the volume determined by a Micromeritics AccuPyc helium porosimeter. Lab procedures are described in more detail by Weger, Eberli [9]. Gas permeability values were obtained from a third-party service company measured at 20 bar and subsequently Klinkenberg-corrected and reported in millidarcies. Permeability measurements were provided from third party service providers.

Ultrasonic velocities measurements on fully brine-saturated samples were performed at center frequencies of 1 MHz using a transmitter–receiver pair that can measure both compressional velocity and two perpendicular shear waves simultaneously with the pulse transmission technique as described in Birch [37]. Pore-fluid pressure was kept constant at 2 MPa while confining pressure was varied to achieve a series of effective pressure conditions (e.g., 5, 10, 15, 20, 25, 30, 35, 40, 45, 50 MPa). The experimental setup is described in more detail in Baechle, Eberli [38] and Weger, Eberli [9]. Most sample sets were measured in pressure steps of 10 MPa to a maximum of 50 MPa effective pressure. However, not all datasets were measured at the same pressure sequence, some used pressure steps of 5 MPa while others used pressure steps of 10 MPa. The maximum pressure used in each dataset was determined by the structural integrity of the samples and as a result, not all datasets could be measured up to the same maximum pressure. Some datasets were measured up to a maximum effective pressure of 80 MPa while others could only be measured up to a maximum effective pressure of 30 MPa. Sample measurements that showed signs of damage through either abrupt velocity increases or a measurable decrease in sample length were discarded.

3.2. Digital Image Analysis

A thin section was prepared from the cut-off of each plug used for the petrophysical measurements. The pore network geometry was assessed with digital image analysis (DIA) from microphotographs of these thin sections. Our DIA is a three-step procedure consisting of image acquisition, image segmentation, and subsequent calculation of pore geometry parameters. We acquired all photomicrographs at a resolution of approximately 6 μm/pixel using a conventional digital camera mounted on an optical light microscope. A combination of color and extinction behavior during rotation under cross-polarized light was used to segment the images into pore space and rock prior to calculate a variety of different geometrical parameters (see [9] for more details on this method). A variety of previous

studies have shown that differences in pore geometry can be most adequately captured by the quantitative pore shape parameters perimeter over area (PoA) and dominant pore size (DomSize) [34,39–42].

PoA is defined as the ratio between the total observed pore-space area on a thin section and the total perimeter that encloses the pore space [43]. It can be considered as the two-dimensional equivalent of specific surface defined as pore volume over pore surface area [32]. Large values of PoA indicate more complex pore structures while smaller PoA values are an indication of simple geometry. DomSize measures the size fraction that dominates a sample and is defined as the upper boundary of equivalent pore diameter of which 50% of the porosity on a thin section is composed [43]. Due to their log-normal distribution, parameter values are often shown as $\log_{10}(\text{PoA})$ and $\log_{10}(\text{DomSize})$ for plotting instead of PoA and DomSize directly.

3.3. Internal Geometry from Specific Surface

Kozeny [32] provides an equation to calculate the effective specific surface from porosity and Klinkenberg permeability,

$$K = \frac{c\varphi^3}{S^2} \tag{1}$$

where and S is the effective specific surface with respect to bulk volume (in m^{-1}) and c is Kozeny's factor calculated as described by Mortensen, Engstrøm [44]

$$c = 1 / \left(4\cos\left(\frac{1}{3}\arccos\left(\varphi\frac{64}{\pi^3} - 1 \right) + \frac{4}{3}\pi \right) + 4 \right) \tag{2}$$

Fabricius, Baechle [31] used specific surface calculated with respect to solid volume,

$$S_g = S / (1 - \varphi) \tag{3}$$

to establish a relationship to VpVs ratio. However, here we will focus more on specific surface calculated with respect to pore volume:

$$S_p = S / \varphi \tag{4}$$

Mortensen, Engstrøm [44] provides information regarding internal pore geometry.

3.4. Extended Biot Theory

Sun [45] introduced a connectivity tensor concept for poro-elasticity similar to the concept of stress tensors for elasticity used by Cauchy in the 1820s. This approach allowed for the development of a consistent general theory of structural media from the first principles of energy conservation. He constructed this model by volume-averaging individual microscopic wave fields that interact with each other at a larger scale [46]. He provided a mathematical representation of the internal structure of porous media by focusing on the geometrical properties of an object that remain unchanged during deformation.

The resulting extended Biot theory (EBT) is a characterization of structural porous media, based on topological characterization, fully compliant with both the Gassmann and Biot theories. It uses both topological and phenomenological parameters to describe physical properties of rocks [45]. In its simplified form the model expresses velocity in terms of porosity, moduli (both bulk and shear), and density of both solid and fluid components and the two topological pore shape parameters f_k (frame flexibility factor) and γ_k (coupling factor) [47]. Both capture different aspects of how pore geometry affects elastic properties in parameterized form [34,43]. Because both parameters are related to the pore shape, these parameters are also related to permeability [34]. Appendix A lists the governing equations of the extended Biot theory.

Calculation of EBT parameter requires basic properties for both minerals and pore fluid as inputs. For density and both bulk and shear modulus of calcite and dolomite we used values summarized by Mavko, Mukerji [24], where compressional velocity for calcite is about Vp_c = 6450 m/s and shear velocity is about Vs_c = 3368 m/s while compressional velocity for dolomite is about Vp_d = 7200 m/s, and shear velocity for dolomite is about Vs_d = 3860 m/s. Bulk densities for dolomite and calcite are given as ρs_c = 2.71 g/cm^3 and ρs_d = 2.87 g/cm^3, respectively. Since pore fluid (32 ppt sodium chloride solution) properties are difficult to determine in a laboratory setting, published values of brine properties from Kleis and Sanchez [48] who provide a compressional velocity of Vp_w = 1430 m/s and a density of ρ_w = 1.03 g/cm^3 were used.

4. Results

4.1. Velocity–Pressure

The compressional velocities of most brine-saturated samples in this study show a high initial velocity increase with increasing pressure at low pressures but become more stable at effective pressures at and above ~20 MPa (Table 1; Figure 3). At low pressure, a pronounced increase in mean velocity change per MPa of 0.00173%/MPa can be observed below ~20 MPa in both dolomite and limestone samples. Measurements above 20 MPa only show a mean velocity change per MPa of 0.00083%/MPa.
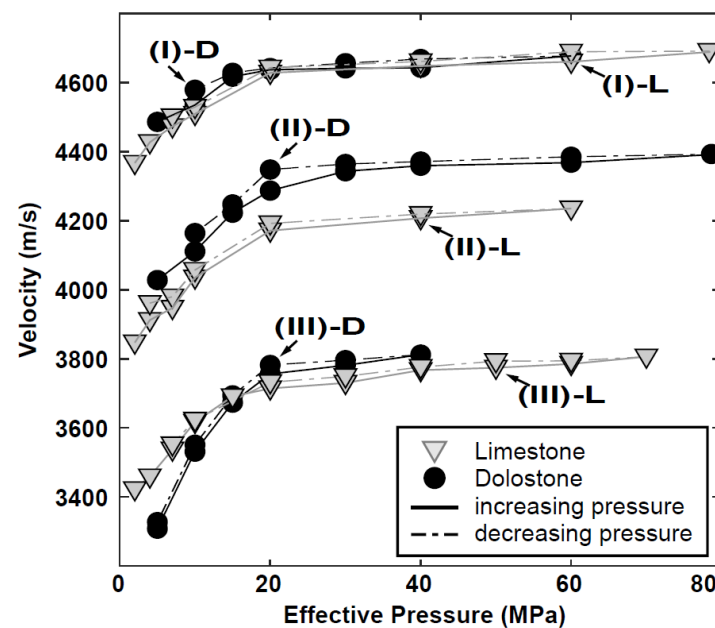
Figure 3. Cross-plot of compressional velocity vs. effective pressure of three pairs of dolomite and limestone with similar porosity for which DIA parameters, EBT parameter γ_k, and permeability measurements are also available. For all samples, dolomites and calcites alike, steady velocity increase with increasing pressure can be observed up to ~20 MPa, after which compressional velocity remains nearly stable (more details on samples I, II, III D & L is provided below).

Since otherwise no discernable differences in the overall velocity–pressure relationship of limestones and dolomites with similar porosity have been observed, we use 20 MPa measurements for further analysis of this study.

Table 1. Basic Statistics (maximum, minimum, mean) of the compressional velocity 40 MPa and the velocity difference between 20 and 40 MPa for all samples in this study.

	# of Samples	Vp (m/s)	δVp (m/s)
		Mean [Min–Max]	(20–40 MPa)
Leg 194 (Neogene)	24	5215 [3925–6153]	59 [4–194]
Turkey (Miocene)	57	5051 [3921–5936]	51 [2–198]
ME #1 (Cretaceous)	78	4151 [2667–6248]	69 [1–153]
ME #2 (Cretaceous)	20	4174 [3390–5638]	68 [6–159]
Madison Fm (Mississippian)	27	5554 [3812–6887]	65 [3–192]
Dolomites	36	5481 [3812–6887]	71 [3–194]
Limestones	170	4547 [2667–6248]	60 [1–198]
Total	206	4710 [2667–6887]	62 [1–198]

4.2. Porosity–Velocity

The porosity measurements of the entire dataset are reasonably uniformly distributed between 0.7% and 33.9% with a mean porosity of 18.5%. Limestones overall show slightly higher porosity with a mean of 20.3% while dolomites have on average a value of 14.8%. The compressional velocity of brine-saturated limestone and dolomite plug samples that were measured at 20 MPa effective pressure ranges from 2658 m/s to 6907 m/s. Dolomites range from 3668 m/s to 6907 m/s while limestones range from 2658 m/s to 6243 m/s (Table 2). A strong first order dependency on porosity can be observed in both datasets (Figure 4). Shear velocities measured at 20 MPa confining pressure range from 1434 m/s to 3760 m/s; where dolomites range from 2072 m/s to 3760 m/s and limestones range from 1434 m/s to 3702 m/s (Table 2). Linear correlations between compressional velocity and porosity based on the limestone and the dolomite data separately result in two slightly different correlation lines with Pearson correlation coefficients $r_l = -0.89$ and $r_d = -0.8$, respectively (both with *p*-values < 0.001). Qualitatively, no discernable difference appears to exist between the velocity measurements of limestone vs. those of dolomite samples. Statistical hypothesis testing reveals that no statistically significant difference between the two correlations exists (F = 11.44, *p* = 0.0008).

Table 2. Basic Statistics (maximum, minimum, mean) of the acoustic velocity measurements at 20 MPa and porosity for all dolomites and limestones used in this study.

	# of Samples	Vp (m/s)	Vs (m/s)	VpVs Ratio	Phi (%)
		Mean [Min–Max]	Mean [Min–Max]	(-)	Mean [Min–Max]
Leg 194 (Neogene)	25	5187 [3907–6080]	2723 [1820–3286]	1.92	20.7 [10.1–32.7]
Leg 359 (Neogene)	35	4481 [3122–6077]	2461 [1699–3674]	1.83	24.7 [8–33]
Turkey (Miocene)	58	5018 [3833–6042]	2872 [2089–3534]	1.76	15.2 [8.2–24.3]
ME #1 (Cretaceous)	78	4083 [2658–6243]	2230 [1479–3223]	1.83	20.5 [0.8–32.3]
ME #2 (Cretaceous)	38	4034 [3262–5514]	2165 [1685–2740]	1.87	24.5 [12.1–31.5]
Maiella (Cretaceous)	38	4174 [3092–5639]	2226 [1549–3209]	1.88	21.4 [4.4–33.9]
ME #3 (Permian)	57	5249 [3668–6637]	2930 [2334–3497]	1.79	13.7 [2.5–31.4]
Madison Fm (Mississippian)	39	5619 [3756–6802]	3084 [2229–3733]	1.82	11.6 [2.2–29.4]
Dolomites	120	5341 [3668–6802]	2949 [2072–3733]	1.81	14.9 [2.2–33]
Limestones	248	4376 [2658–6243]	2399 [1479–3534]	1.83	20.4 [0.8–33.9]
Total	368	4691 [2658–6802]	2579 [1479–3733]	1.83	18.6 [0.8–33.9]
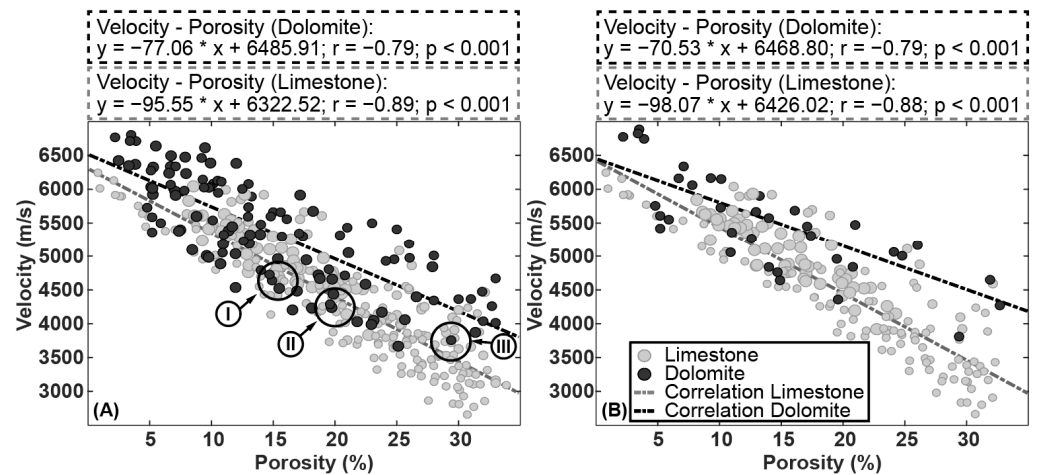
Figure 4. Compressional velocity vs. porosity of limestone and dolomite samples under fully saturated conditions and measured at (**A**) 20 MPa and (**B**) 40 MPa effective pressure. Only a minor increase in velocity (mean $\delta V_{P(20-40MPa)}$ = 62.3 m/s) is observed between the velocity at 20 MPa versus 40 MPa (see Table 1). A relationship between velocity and porosity exists, but large scatter dominates both datasets. No substantial difference is observed between dolomite and limestone samples. Circles indicate the samples for which photomicrographs are shown in Figure 10.

4.3. VpVs Ratio

VpVs ratios of the samples in this study range from 1.49 to 2.25 with a mean of 1.83. No discernable difference can be detected between dolomites and limestones which range from 1.49 to 2.12 with a mean of 1.81 and from 1.5 to 2.25 with a mean of 1.83, respectively. No statistically significant correlation could be established between VpVs ratio and porosity for limestones (R = −0.09, *p* = 0.18) and only a very weak correlation exists for dolomites (R = −0.23, *p* < 0.01). As a result, detrending VpVs ratio from porosity as suggested by Fabricius, Baechle [34] seems superfluous. Even at low confidence (e.g., 90%) correlation bounds to predict a new observation based on the dolostone sample regression between VpVs ratio and porosity are almost fully inclusive of the limestone samples (Figure 5).
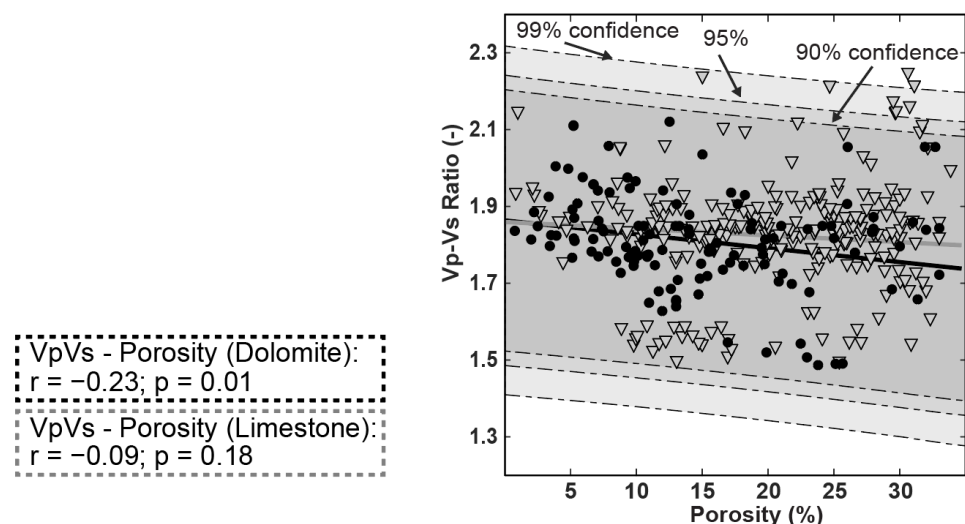
Figure 5. VpVs ratio versus porosity measurements showing no significant difference exists between dolostone and limestones. Prediction bounds for new observation based on the dolostone samples (superimposed in gray) are almost fully inclusive of the limestone dataset.

4.4. Quantitative Pore-Shape Parameters from Digital Image Analysis (DIA)

We derived the DIA parameters DomSize and PoA for a total of 243 samples (148 limestones and 95 dolomites). The PoA values of the entire dataset range from 17 mm^{-1} to 543 mm^{-1} with a mean of ~135 mm^{-1} (Figure 6). PoA values measured on dolomite samples range from 19 mm^{-1} to 543 mm^{-1} while PoA values measured on limestone samples range from 19 mm^{-1} to only $\leq$543 mm^{-1}, with mean PoA values of dolomite and limestone at 167 mm^{-1} and 115 mm^{-1}, respectively. DomSize of the entire dataset, as equivalent diameter, ranges from 20 μm to 891 μm, with a mean of 181 μm. DomSize of dolomite samples ranges from 23 μm to 642 μm (mean = 156 μm) while DomSize of limestone samples ranges from 20 μm to 891 μm (mean = 196 μm). Both PoA and DomSize show an approximate rational functional relationship (Figure 6). The dolomite samples of this study have smaller DomSize and larger PoA than the limestone samples which are dominated by larger, less complicated pores (Table 3).
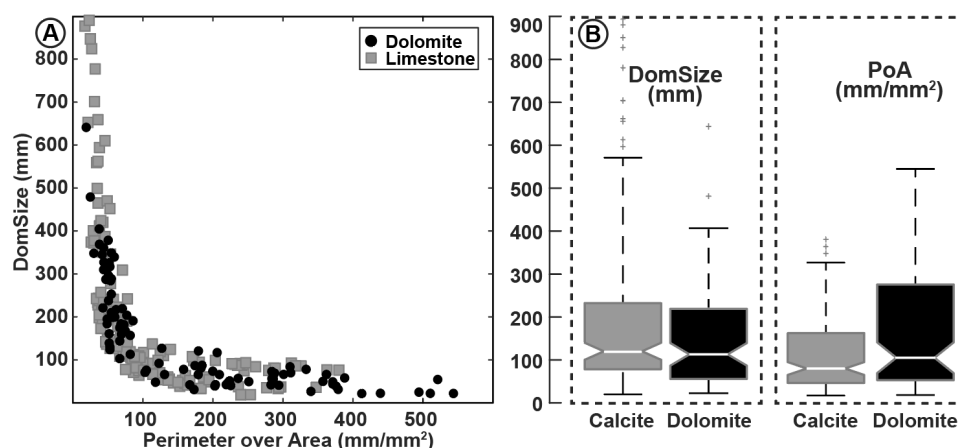
Figure 6. (**A**) Cross-plot of perimeter over area (PoA) vs. dominant size (DomSize) of dolomite and limestone samples. (**B**) Box plots of PoA vs. DomSize for dolomite and limestone samples. Dolomites contain overall smaller, more complex pores with larger PoA, while limestones tend to have larger, simpler pores with lower PoA.

Table 3. Basic statistics (maximum, minimum, mean) of DIA parameters PoA and DomSize for all dolomites and limestones used in this study.

	# of	PoA (mm^{-1})	DomSize (mm)
	Samples DIA	Mean [Min–Max]	Mean [Min–Max]
Leg 194 (Neogene)	22	47 [25–77]	394 [205–702]
Leg 359 (Neogene)	3	127 [66–194]	101 [55–148]
Turkey (Miocene)	38	202 [29–380]	113 [34–401]
ME #2 (Cretaceous)	38	81 [25–240]	244 [20–848]
Maiella (Cretaceous)	36	93 [38–254]	108 [20–224]
ME #3 (Permian)	34	229 [38–543]	113 [23–406]
Madison Fm (Mississippian)	38	138 [30–494]	146 [26–349]
Dolomites	95	167 [19–543]	156 [23–642]
Limestones	148	115 [17–380]	196 [20–891]
Total	243	135 [17–543]	181 [20–891]

4.5. Porosity and Compressional Velocity in the Context of Extended Biot Theory

The EBT pore shape parameter γ_k was calculated for both dolomites and calcites. The γ_k values range from 1.3 to 8.3 where dolomite shows overall higher values ranging from 2.0 to 8.3 (Figure 7B) while calcite values range between 1.3 and 6.7 (Figure 7A). Calculated coupling factor γ_k varies under changing velocity and porosity (Figure 7 background

contour lines). Values of γ_k are higher at low compressional velocity and lower at high compressional velocities at any given porosity and regardless of mineralogy. Lines of constant γ_k are sloped diagonally (~45° from top left to bottom right in velocity–porosity space), indicating that γ_k is much less dependent on velocity and porosity values individually but a combination of both.
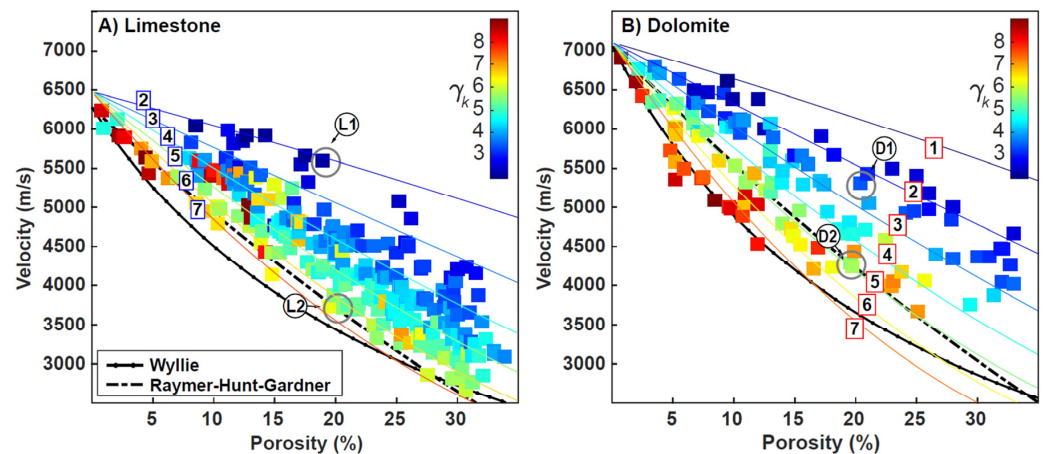

Figure 7. Compressional velocity–porosity cross-plots of limestone (**A**) and dolomite (**B**) samples. The calculated coupling factors are plotted in colored squares and the contour lines of the theoretical coupling factor γ_k are superimposed. At any given porosity, samples with high velocity have a low coupling factor γ_k and samples with low velocity have a high coupling factor γ_k. Blue and Red numbers on contour lines represent theoretical values of γ_k for calcite and dolomite respectively. Gray circles indicate thin sections discussed in Section 5.1.

Lower values of γ_k at any given porosity indicate better coupling and characterize stiffer rocks with higher velocity for their porosity and mineralogy. In the data presented here, the limestone samples show overall lower values of γ_k than the dolomites and, regardless of mineralogy, the values calculated from measurements correspond well with the theoretical contour lines of γ_k for a wide range of porosity and velocity (Figure 7).
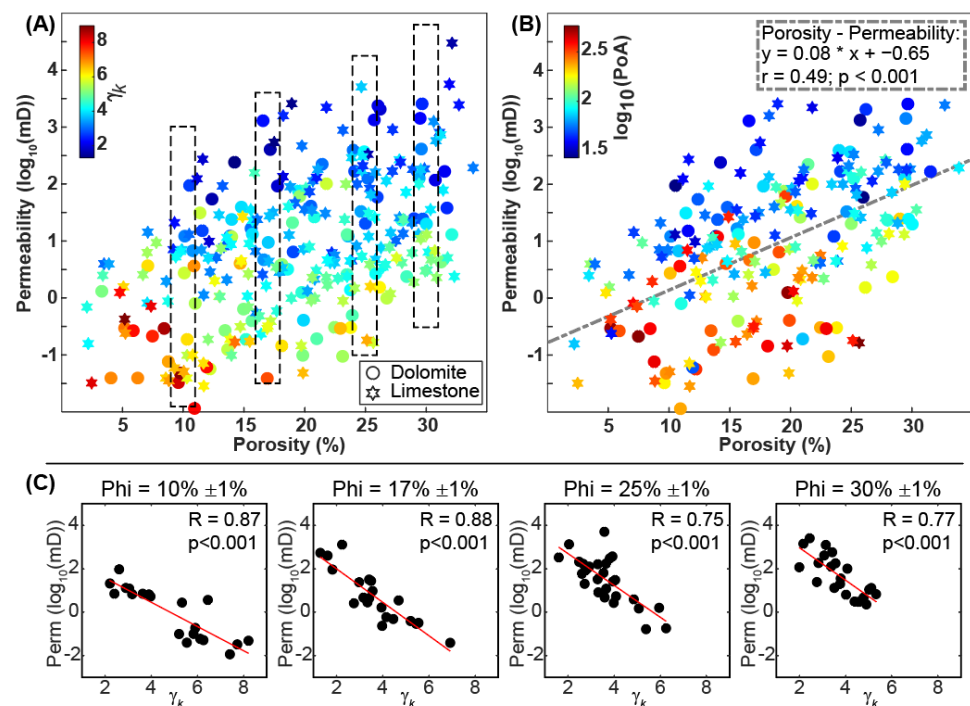
4.6. Permeability

Permeability was measured for 289 samples (204 limestones and 95 dolomites). The values range from 0.1 mD to 29,369 mD with limestone samples showing higher permeabilities than dolomite samples (Table 4, Figure 8). As commonly seen in carbonate reservoir rocks, the direct relationship between porosity and permeability is very poorly defined (Figure 8). Direct linear correlation between porosity and permeability does not yield statistical significance with a correlation coefficient of only 0.49 and a *p*-value of $p < 0.001$ but, regardless of mineralogy, low-permeability samples are characterized by low specific surface values.

Overall, samples with relatively low permeability for their porosity display higher values of PoA, characterizing more complex pore systems often dominated by smaller pores. In contrast, samples with relatively high permeability for their porosity are dominated by lower values of PoA, representing less complex pore systems with often larger, more spherical pores (Figure 9B). Similarly, samples with a low coupling factor γ_k, at any given porosity, show higher permeabilities than samples with higher coupling factor γ_k (Figure 9A,C).
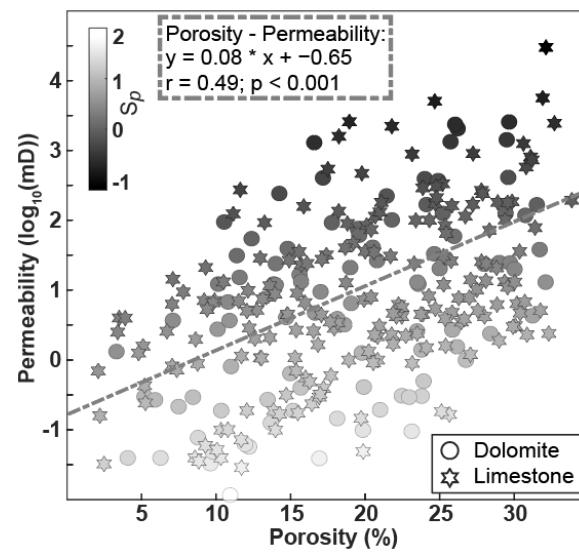
Figure 8. Permeability vs. porosity cross-plot of limestone and dolomite samples. The specific surface with respect to pore volume as defined by Mortensen et al. (1998) [44] is superimposed in shades of gray.

Figure 9. Permeability vs. porosity of limestone and dolostone samples showing substantial variability of permeability at any given porosity and no well-defined correlation exists. Superimposed in color are the EBT parameter γ_k (**A**) and in (**B**) PoA, the 2D equivalent of specific surface. Higher values of PoA, representing smaller, more complex pore systems, are more abundant in samples with lower permeabilities at a given porosity range, while lower values of PoA, representing larger, more spherical, and less complex pore systems are more abundant in samples with higher permeability for their given porosity. A similar relationship exists for the EBT parameter γ_k. (**C**) Correlations between permeability and γ_k within small ranges of porosity (dashed boxes in (**A**) illustrate that low permeability and γ_k are inversely correlated).

Table 4. Basic statistics (maximum, minimum, mean) of permeability measurements, the EBT coupling factor γ_k, and specific surface with respect to pore volume as defined by Mortensen et al. (1998) [44] for all dolomites and limestones used in this study.

	# of	K (mD)	γk (-)	Sp (m²/cm³)
	Samples Perm	**Mean [Min–Max]**	**Mean [Min–Max]**	**Mean [Min–Max]**
Leg 194 (Neogene)	25	2139 [12.2–29369]	2.1 [1.3–3.6]	0.6 [0.07–2.01]
Leg 359 (Neogene)	4	11 [0.2–25]	3.2 [2.6–4.5]	9.87 [2.39–22.87]
Turkey (Miocene)	43	37 [0.03–1281]	4.1 [2.2–6.4]	10.38 [0.25–44.19]
ME #1 (Cretaceous)	69	133 [0.04–5000]	4.5 [2–6.5]	8.88 [0.15–35.4]
ME #2 (Cretaceous)	38	144 [1.55–2195]	3.6 [1.9–5.7]	2.93 [0.22–9.05]
Maiella (Cretaceous)	36	124 [0.17–725]	3.4 [2.6–6.7]	2.91 [0.46–20.18]
ME #3 (Permian)	36	21 [0.01–240]	5.6 [2–8.2]	17.53 [0.75–67.26]
Madison Fm (Mississippian)	38	18 [0.16–101]	4.4 [2.2–8.3]	3.26 [1.12–10.3]
Dolomites	84	149 [0.01–5564]	4.7 [2–8.3]	9.08 [0.17–67.26]
Limestones	205	308 [0.03–29369]	3.8 [1.3–6.7]	6.45 [0.07–44.19]
Total	289	262 [0.01–29369]	4.1 [1.3–8.3]	7.21 [0.07–67.26]

4.7. Specific Surface

In our samples, values of specific surface with respect to pore volume (S_p) range from $0.07 \text{ m}^2/\text{cm}^3$ to $67.26 \text{ m}^2/\text{cm}^3$ with a mean of $7.43 \text{ m}^2/\text{cm}^3$. Dolomites show overall higher values with a mean of $9.25 \text{ m}^2/\text{cm}^3$, ranging from $0.17 \text{ m}^2/\text{cm}^3$ to $67.26 \text{ m}^2/\text{cm}^3$, while limestone values average only $6.69 \text{ m}^2/\text{cm}^3$, ranging from $0.07 \text{ m}^2/\text{cm}^3$ to $45.99 \text{ m}^2/\text{cm}^3$ (Table 4).

Fabricius et al. (2007) [33] related the $\log_{10}$ of specific surface with respect to solid volume (S_d) to detrended VpVs ratio to estimate permeability. The link between specific surface and VpVs ratio implies that VpVs ratio can quantify, to some extent, internal pore geometry of the sample. Performing the same analysis with our samples a correlation between $\log_{10}(Sg)$ and VpVs ratio results in a Pearson correlation coefficient R = −0.55 ($p < 0.001$).

To evaluate how much insight into internal pore geometry can be provided by theoretically calculated specific surface in the first place, we compare thin-section-derived parameter PoA with S_p, specific surface with respect to pore volume, and the correlation for all samples in this study between $\log_{10}(S_p)$ and $\log_{10}(PoA)$ results in a Pearson correlation coefficient of R = 0.69 ($p < 0.001$), indicating a somewhat stronger link between PoA and S_p.

Correlation between EBT parameter γ_k derived from acoustic measurements and $\log_{10}(S_p)$ results in an even stronger Pearson correlation coefficient of R = 0.73 ($p < 0.001$), indicating a well-established link between specific surface and the coupling factor γ_k.

5. Discussion

5.1. Porosity Types in Limestone and Dolomite

Most dolostones in this study are composed of fabric destructive dolomite with crystal sizes ranging from ~10 μm to ~100 μm. Only in some of the samples are the remains of the original texture visible, but even those samples are dominated by dolomite crystal contacts and intercrystalline porosity. The limestone samples of highly variable grain size are predominantly composed of skeletal packstone, grainstone, and a few wackestone textures and contain mainly inter- and intraparticle porosity.

Thin sections of three sample pairs (locations indicated as circles in Figure 4A) consisting each of one dolostone and one limestone with similar velocity and porosity values illustrate variations in texture and pore structure in these pairs (Figure 10). In sample set I (Figure 10 top) dolostone and limestone both have approximately 15% porosity and a measured compressional velocity of approximately 4600 m/s. The limestone sample is a coarse skeletal grainstone containing large rudist fragments and has mostly large and overall simple pores.
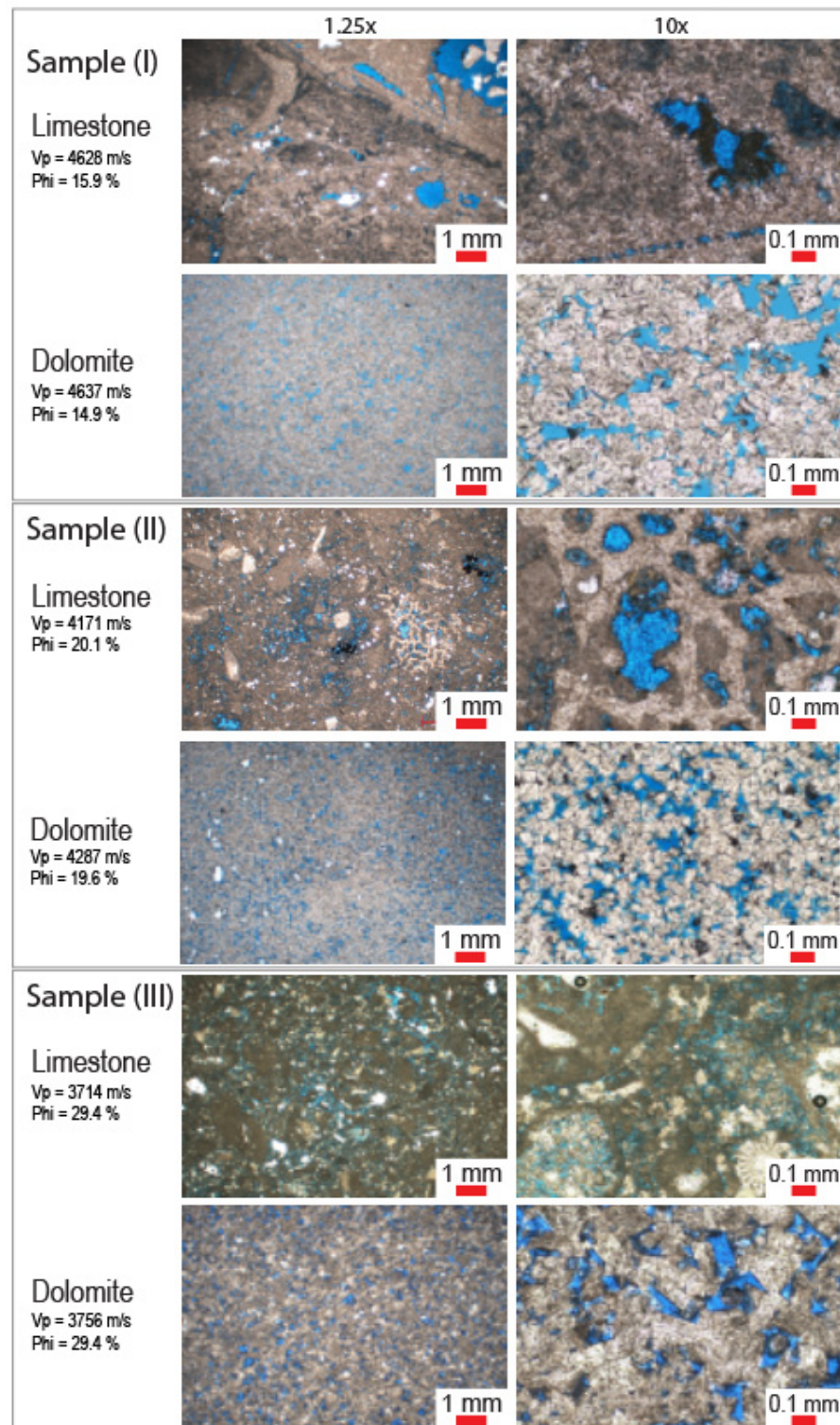
Figure 10. Thin section images of the limestone and dolostone samples I, II, and III. All three samples show similar porosity–velocity values (see Figure 4). Dolostones are consistently crystalline rocks with intercrystalline porosity of varying pore sizes while limestones are mainly wackestone to grainstone dominated by inter- and intraparticle porosity with some proportion of microporosity.
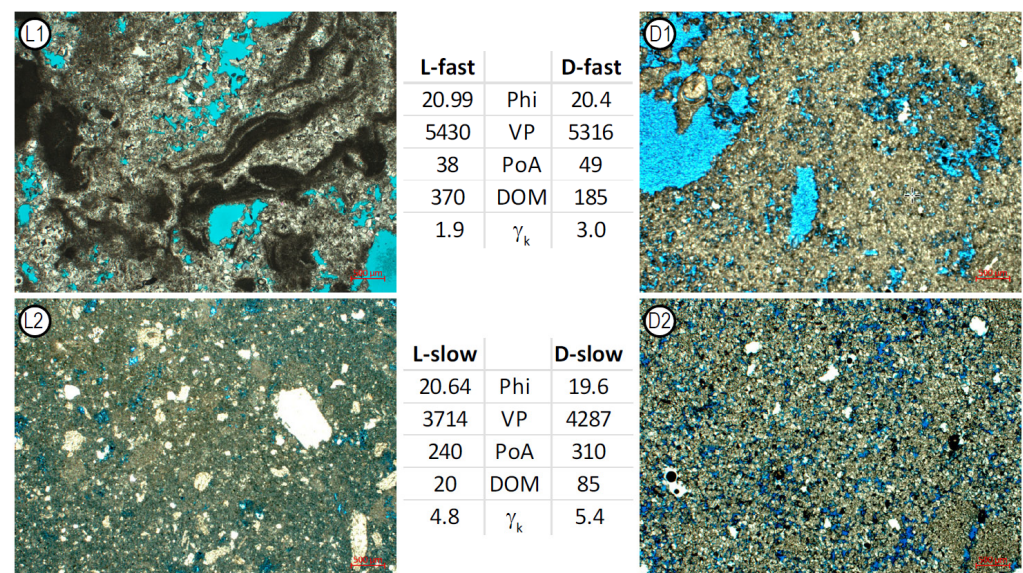
The limestone shows mostly intraparticle and some interparticle porosity. The dolostone, however, is composed of uniform dolomite crystals of approximately 30–100 μm in size producing a uniform intercrystalline porosity. In sample set II (Figure 10 center) porosity is ~20% with a measured compressional velocity of approximately 4250 m/s.

The limestone sample is a wackestone to packstone containing large skeletal fragments surrounded by finer grained, silt to mud-sized matrix. Most porosity here is interparticle but some intraparticle porosity remains. Just as in sample set I, the dolostone of set II shows fabric destructive dolomitization with only slightly more patchy porosity distribution than the samples in set I. The dolomite sample is dominated by smaller crystals of 10–60 μm and similar pore sizes. In sample set III (Figure 10 bottom) porosities are approximately 30% with a measured compressional velocity of approximately 3750 m/s. The limestone sample is a skeletal peloidal grainstone containing large fragments (>1 mm) surrounded by very little mud-sized material. Most porosity is interparticle but some intraparticle porosity remains. Some recrystallization can be observed within some of the skeletal fragments. In all three examples the limestones are composed of larger particles showing larger and simpler pores while the dolomites are created by fabric destructive dolomitization that created rocks composed of small crystals (10–100 μm) and intercrystalline porosity creating a complex network of small pores.

5.2. Velocity–Porosity Relationship

Cross-plots of compressional velocity vs. porosity of carbonate rock samples always tend to show large velocity variability at any given porosity. This variability is generally attributed to changes in pore type or internal pore geometry [7,9,11,20,38,49]. The samples analyzed in this study show an extremely large spread in velocity–porosity space (Figure 4). Samples with nearly the same velocity show porosities that vary by as much as 20% (Figure 4), and samples with the same porosity often vary in sonic velocity by more than 1400 m/s. Although large in appearance, the variations documented in the samples of this study are smaller than those observed by Anselmetti and Eberli [14] in the dataset of mixed mineralogy (dolomites and calcites) from the Bahama Drilling Project.

To further illustrate the effect of pore geometry on acoustic velocity we selected thin section photomicrographs from four specific samples, two dolomites and two limestones, with similar porosity (~20%–21%) for detailed comparison (Figure 11).

L-fast		D-fast
20.99	Phi	20.4
5430	VP	5316
38	PoA	49
370	DOM	185
1.9	γ_k	3.0

L-slow		D-slow
20.64	Phi	19.6
3714	VP	4287
240	PoA	310
20	DOM	85
4.8	γ_k	5.4

Figure 11. Photomicrographs of limestone samples L1 and L2 and dolomite samples D1 and D2 with their corresponding measured properties. The differences in pore geometry and physical properties between the top row (L1 and D1) and the bottom row (L2 and D2) illustrate the observed differences between fast and slow rocks with ~20% porosity are related to the pore shape parameters and γk. See Figure 7 for samples' location within velocity–porosity space. (see Figure 7 for sample properties in context of the entire dataset).

The four samples represent the high- and low-velocity endmembers at ~20% porosity for dolomite and limestone samples from this study. The samples' position in velocity–porosity space can be seen in Figure 7 where the samples are marked as L1, L2, D1, and D2. Figure 11 shows thin section photomicrographs and the samples' measured values of porosity, compressional velocity, PoA, DomSize, and γ_k. Samples L1 and D1 (Figure 11) show relatively high velocity for their porosity. They are dominated by large pores (DomSize $\geq$ 185) with simple internal geometry (PoA $\leq$ 50). Both show relatively low γ_k, where that of the dolomite sample D1 is somewhat higher (γ_k = 3.0) than the limestone sample L1 (γ_k = 1.9). In contrast, samples L2 and D2 (Figure 11) show relatively low velocity for their porosity. Both samples are dominated by a larger number of small pores (DomSize $\leq$ 85) containing both interparticle and microporosity and their internal geometry is more complex with larger values of specific surface (PoA $\geq$ 240); a combination conducive for low velocity [9,34]. The two samples with relative low velocity for their given porosity show relatively low values of coupling factor γ_k, where that of the dolomite sample D2 is somewhat higher (γ_k = 5.4) and that of the limestone sample L1 is somewhat lower (γ_k = 4.8).

Overall, all limestone samples display predominantly grainstone to packstone texture with pore geometries that include intra- and interparticle and some microporosity. They contain less abundant and larger pores, a geometry conducive to higher velocities [9,34]. Moreover, many of the analyzed samples indicate that diagenetic alteration had strengthened grain to grain contacts by fusing them together by means of micritic meniscus-type cement as described by Hillgärtner, Dupraz [50] and Diaz, Eberli [51]. Such cemented grain to grain contact provides the means for acoustic wave propagation at velocities higher than expected for the given mineral composition.

Their dolomite counterparts that exhibit very similar compressional velocities are dominated by textures of sucrosic dolomite with pore geometries dominated by a large amount of small interparticle porosity, a combination conducive for lower velocity [9,34]. Variation in compressional velocity at a given porosity is partially due to fact that dolomite is denser and has higher bulk modulus than calcite as illustrated eloquently by Wyllie, Gregory [52].

5.3. The Impact of Mineral Velocity

Mavko, Mukerji [24] summarized moduli and density of common minerals and show five different published results for calcite properties ranging from 6260 m/s to 6640 m/s [26,28,29,53,54] and three for dolomite ranging from 6930 m/s to 7340 m/s [55–57]. In addition to those results, Chen, Lin [58] determined the single-crystal elastic moduli of calcite using Brillouin spectroscopy under ambient conditions, resulting in a compressional velocity of 6640 m/s. Dandekar [59] found elastic properties of calcite at ambient temperatures to be slightly higher than those that he published previously [26]), resulting in compressional velocity of 6603 m/s. Hearmon [60]) and Vo Thanh and Lacam [61]) both determined single-crystal elastic properties of calcite that result in compressional velocities in excess of 6500 m/s (6532 m/s and 6577 m/s, respectively). In summary, published values for compressional velocity of single-crystal calcite are on average 6480 m/s; about 630 m/s slower than the compressional velocity resulting from published values for single-crystal dolomites which average at 7110 m/s.

Confidence bounds for a given correlation can visually illustrate the range of velocity–porosity values one might expect when attempting to predict new observations based on an underlying sample regression. For the data in this study, both regressions (dolostone and limestone) produce confidence bounds and corresponding intervals (at 90%, 95%, and 99%) that are inclusive of all the samples in this study regardless of mineralogy. For example, all limestone samples from this study fall well within the confidence intervals based on the dolomite data regression that bound the range within which the new dolomite porosity–velocity prediction is expected to fall (Figure 12).
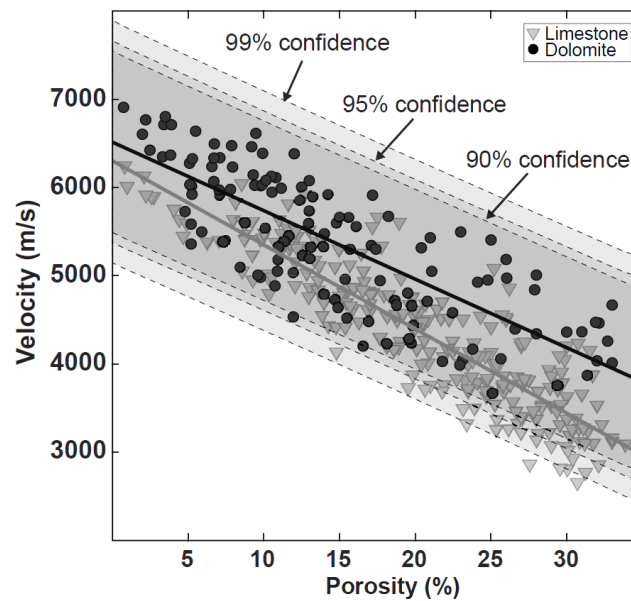
Figure 12. Compressional velocity vs. porosity of water-saturated limestone and dolomite samples measured at 20 MPa confining pressure. Correlation bounds to predict a new observation based on the dolostone sample regression are superimposed in gray. Note that dolomite-based correlation bounds are fully inclusive of the limestone dataset.

5.4. The Importance of Internal Geometry

Digital image analysis as well as the theoretical coupling factor γ_k from the extended Biot theory provides the means to distinguish rocks with pore geometries conducive for higher velocity from those dominated by geometries conducive for lower velocities (Figure 7). At the same time, both DIA and the extended Biot theory parameter allow for the separation of rocks with higher permeability from those with lower permeability (Figure 9) [33].

Higher values of coupling factor γ_k are indicative of a complex internal pore network dominated by large numbers of small pores (high PoA and low DomSize) conducive to lower velocity and lower permeability. Lower values of coupling factor γ_k are indicative of simpler pore networks composed of larger pores conducive to higher velocity and higher permeability (Figures 7 and 8). Regardless of matrix mineralogy, samples with geometries more commonly found in grainstone, floatstone, and/or rudstone or floatstone containing large interparticle, intraparticle, moldic, and/or vuggy pores (Figure 13A) tend to exhibit higher velocities for the given base elastic properties of their matrix minerals. In contrast, samples with internal pore structures more frequently observed in mudstone, wackestone, packstone, or fully recrystallized pure crystalline rocks containing predominantly small interparticle porosity (Figure 13B) generally show lower velocities for the given base elastic properties of their matrix minerals.

The dolomites measured for this study all show values of coupling factor γ_k that are notably higher than for limestones of comparable velocity–porosity (Figure 5, Table 1). The pore structures observed in the dolomites from this study follow the geometrical pattern of those rocks showing lower velocities for the given base elastic properties (Figure 13B) while most limestones from this study show internal pore geometries like those found frequently in rocks that tend to exhibit higher velocities for the given base elastic properties (Figure 13A). In summary, the internal geometry of the dolomite samples from this study provides a weaker framework that compensates for the stiffer elastic properties of their matrix mineral, while the internal geometry of the limestone samples from this study provides a stiffer framework capable of compensating for the weaker matrix mineral properties of calcite.
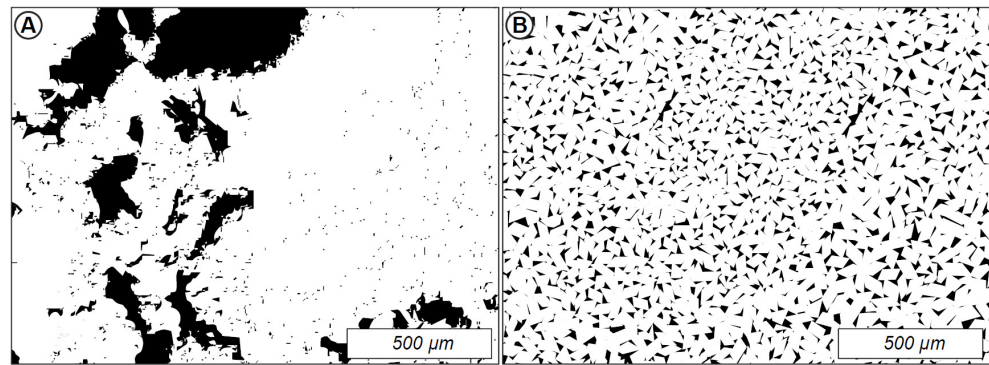
Figure 13. (**A**) Binarized thin section photomicrograph of a sample with small number of large pores, low PoA, and low γ_k (sample L1); representative for fast geometries commonly found in grainstone, floatstone, and/or rudstone containing large interparticle, intraparticle, moldic, and/or vuggy pores. (**B**) Binarized thin section photomicrograph of a sample with large number of small pores, high PoA, and high γ_k (Sample D2); representative for slow geometry more frequently observed in mudstone, wackestone, packstone, or fully recrystallized pure crystalline rocks containing predominantly small interparticle porosity.

6. Conclusions

The comparison of acoustic measurements from 247 limestone and 123 dolomite samples shows that all 370 carbonate samples occupy essentially the same range of velocity–porosity values (Figures 2 and 5). Based on statistical hypothesis testing we conclude that there is no statistically significant difference in velocity–porosity between the dolomite and the limestone samples (Figure 13). The difference in matrix compressional velocities between dolomite and calcite (e.g., $Vp_d \cong 7110$ m/s and $Vp_c \cong 6480$ m/s) has been determined repeatedly over decades on single crystals and should be considered indisputable. However, the difference between measured matrix velocity of dolomite and calcite is only ~630 m/s, much lower than the velocity variations more than 1000–1500 m/s that are frequently observed in datasets composed of only calcite or dolomite alone.

Moreover, both image parameters and coupling factor γ_k from dolomites and limestones of similar velocity–porosity show that dolomite samples are dominated by pore geometries typical for low velocities (complex geometries and small pore sizes) while comparable limestones are dominated by pore geometries more typically found in samples with high sonic velocity (simple pore networks with large pores).

The observed differences in pore geometry between dolomites and limestones of similar velocity compensate for the difference in matrix velocity. The large velocity variability caused by changes in pore network geometries greatly exceeds the effect of velocity variation between dolomite and limestone. We conclude that the wide range of pore geometries in carbonates often overrides the effects of mineralogy. This finding implies that the estimation of sonic matrix properties from bulk measurements may lead to erroneous results if pore network geometry is not accurately incorporated in the estimation procedures.

More importantly, the EBT coupling factor γ_k that is exclusively extracted from acoustic data can serve as a robust quantitative indicator of pore geometries. γ_k can refine permeability estimates, especially when no other measurements of pore network geometry are available. Use of acoustic-data-derived γ_k can provide a comprehensive understanding of the pore structures and pore geometry of subsurface formations.

7. Implications

A solid understanding of a formation's internal geometry and its fluid flow dynamics are the most basic required building blocks of any reservoir characterization effort. Utilization of γ_k from seismic data could enable engineers and geoscientists to make more accurate predictions of fluid flow dynamics and its special distribution. Both internal geometry and reservoir fluid flow are required when optimizing production strategies or identifying

potential hydrocarbon reservoirs. Furthermore, most carbon capture and storage efforts rely on the ability to assess pore geometries to evaluate feasibility of long-term CO_2 subsurface storage. As a result, the proper use of γ_k may contribute to climate change mitigation efforts. Similarly, in enhanced oil recovery (EOR) projects, the insights provided by γ_k regarding pore space geometries can facilitate the design and implementation of efficient injection strategies to enhance oil recovery rates.

However, deriving pore geometry from acoustic data by means of EBT parameter γ_k has a broader impact on geophysical applications. Its ability to derive meaningful pore geometry information from acoustic data alone streamlines formation characterization processes and reduces the dependency on costly coring and/or time-consuming laboratory measurements. γ_k can be seen as a potential extension to seismic reservoir characterization that could be useful for many other subsurface challenges in mining, construction, and engineering.

The use of γ_k to determine pore geometry and permeability in different geological settings outside the carbonate world and across a wider range of rock types will require further refinement. However, combining γ_k with other geophysical data such as EM and resistivity may lead to more reliable predictive models.

Appendix A

The simplified EBT model presented by Sun et al. (2001) [34] expresses velocity through Equations (A1)–(A10) (for detailed derivations of these equations, see Sun 1994 [47]).

$$V_p = \sqrt{\frac{K + \frac{4}{3}\mu}{\rho}} \tag{A1}$$

$$V_s = \sqrt{\frac{\mu}{\rho}} \tag{A2}$$

$$\rho = (1 - \varphi)\rho_s + \varphi\rho_f \tag{A3}$$

$$K = (1 - \varphi_k)K_s + \varphi_k K_f \tag{A4}$$

$$\varphi_k = F_k \varphi \tag{A5}$$

$$F_k = \frac{1 - (1 - \varphi)f_k}{[1 - (1 - \varphi)f_k]\frac{K_f}{K_s} + \left(1 - \frac{K_f}{K_s}\right)\varphi} \tag{A6}$$

$$\mu = \mu_s(1 - \varphi)f_\mu \tag{A7}$$

$$f_k = (1 - \varphi)^{\gamma_k - 1} \tag{A8}$$

$$f_\mu = (1 - \varphi)^{\gamma_\mu - 1} \tag{A9}$$

where:

V_p = compressional velocity
K_s = bulk modulus of the solid
V_s = shear velocity
K_f = bulk modulus of the fluid
K = bulk modulus
μ_s = shear modulus of the solid
μ = shear modulus
φ = porosity
ρ = bulk density
φ_k = effective porosity
ρ_s = bulk density of the solid
F_k = effective coupling factor
ρ_f = bulk density of the fluid
$f_k, f_\mu, \gamma_k, \gamma_\mu$ = frame flexibility factors

This formulation provides sufficient information so that both topological parameters (f_k and γ_k) can be expressed in terms of known quantities. Some algebraic rearrangement leads to

$$\gamma_k = \frac{\ln\left(\frac{\varphi K(K_f - K_s) - K_f(K - K_s)}{\varphi^2(K_s^2 - K_s K_f) - \varphi(K_s^2 - K_f K) - K_f(K - K_s)}\right)}{\ln(1 - \varphi)} + 1 \tag{A10}$$

In this expression, bulk modulus K can be directly derived from the measured compressional velocity, shear velocity, and porosity. In controlled laboratory experiments where solid and fluid bulk moduli are known, this formulation can be used to calculate γ_k directly from acoustic properties. The parameter f_k can be calculated subsequently using Equation (A8).

References

1. Palaz, I.; Marfurt, K.J. (Eds.) Carbonate Seismology: An Overview. In *Carbonate Seismology*; Society of Exploration Geophysicists: Tulsa, OK, USA, 1997; pp. 1–7.
2. Anselmetti, F.S.; Eberli, G.P. Controls on sonic velocity in carbonates. *Pure Appl. Geophys.* **1993**, *141*, 287–323. [CrossRef]
3. Adam, L.; Batzle, M. Elastic properties of carbonates from laboratory measurements at seismic and ultrasonic frequencies. *Lead. Edge* **2008**, *27*, 1026–1032. [CrossRef]
4. Bashah, N.S.I.; Pierson, B. The impact of pore geometry and microporosity on velocity-porosity relationship in carbonates of central Luconia, Sarawak. In Proceedings of the Adapted from Extended Abstract, AAPG International Conference on Exhibition, Singapore, 16–19 September 2012.
5. Rafavich, F.; Kendall, C.H.S.C.; Todd, T.P. The relationship between acoustic properties and the petrographic character of carbonate rocks. *Geophysics* **1984**, *49*, 1622–1636. [CrossRef]
6. Wang, Z. Seismic properties of carbonate rocks. In *Carbonate Seismology*; Geophysical Development Series; Society of Exploration Geophysicists: Tulsa, OK, USA, 1997; pp. 29–52.
7. Anselmetti, F.S.; Eberli, G.P. Sonic velocity in carbonate sediments and rocks. In *Carbonate Seismology*; Palaz, I., Marfurt, K.J., Eds.; Society of Exploration Geophysicists: Tulsa, OK, USA, 1997; pp. 53–74.
8. Baechle, G.T.; Weger, R.; Eberli, G.; Massaferro, J.L. Pore structure effects on elastic moduli-porosity relationships in carbonate rocks. In Proceedings of the AGU Spring Meeting Abstracts, New Orleans, LA, USA, 24 May 2005.
9. Weger, R.J.; Eberli, G.P.; Baechle, G.T.; Massaferro, J.L.; Sun, Y.-F. Quantification of pore structure and its effect on sonic velocity and permeability in carbonates. *AAPG Bull.* **2009**, *93*, 1297–1317. [CrossRef]
10. Janson, X.; Lucia, F.J. Matrix microcrystalline structure and acoustic properties of oomoldic dolograinstone. Sonic velocity of moldic dolograinstone. *Geophysics* **2018**, *83*, MR199–MR210. [CrossRef]

11. Verwer, K.; Eberli, G.; Baechle, G.; Weger, R. Effect of carbonate pore structure on dynamic shear moduli. *Geophysics* **2010**, *75*, E1–E8. [CrossRef]
12. Borgomano, J.; Pimienta, L.; Fortin, J.; Guéguen, Y. Dispersion and attenuation measurements of the elastic moduli of a dual-porosity limestone. *J. Geophys. Res. Solid Earth* **2017**, *122*, 2690–2711. [CrossRef]
13. Wyllie, M.; Gregory, A.; Gardner, G. An experimental investigation of factors affecting elastic wave velocities in porous media. *Geophysics* **1958**, *23*, 459–493. [CrossRef]
14. Anselmetti, F.S.; Eberli, G.P. The velocity-deviation log: A tool to predict pore type and permeability trends in carbonate drill holes from sonic and porosity or density logs. *Am. Assoc. Pet. Geol. Bull.* **1999**, *83*, 450–466.
15. Wang, Z.Z. Fundamentals of seismic rock physics. *Geophysics* **2001**, *66*, 398–412. [CrossRef]
16. Assefa, S.; McCann, C.; Sothcott, J. Velocities of compressional and shear waves in limestones. *Geophys. Prospect.* **2003**, *51*, 1–13. [CrossRef]
17. Xu, S.; Payne, M.A. Modeling elastic properties in carbonate rocks. *Lead. Edge* **2009**, *28*, 66–74. [CrossRef]
18. Fournier, F.; Leonide, P.; Biscarrat, K.; Gallois, A.; Borgomano, J.; Foubert, A. Elastic properties of microporous cemented grainstones. *Geophysics* **2011**, *76*, E211–E226. [CrossRef]
19. Kenter, J.A.; Braaksma, H.; Verwer, K.; van Lanen, X.M. Acoustic behavior of sedimentary rocks: Geologic properties versus Poisson's ratios. *Lead. Edge* **2007**, *26*, 436–444. [CrossRef]
20. Anselmetti, F.S.; Luthi, S.; Eberli, G.P. Quantitative characterization of carbonate pore systems by digital image analysis. *Am. Assoc. Pet. Geol. Bull.* **1998**, *82*, 1815–1836.
21. Regnet, J.; David, C.; Fortin, J.; Robion, P.; Makhloufi, Y.; Collin, P. Influence of microporosity distribution on the mechanical behavior of oolithic carbonate rocks. *Geomech. Energy Environ.* **2015**, *3*, 11–23. [CrossRef]
22. Regnet, J.B.; Robion, P.; David, C.; Fortin, J.; Brigaud, B.; Yven, B. Acoustic and reservoir properties of microporous carbonate rocks: Implication of micrite particle size and morphology. *J. Geophys. Res. Solid Earth* **2015**, *120*, 790–811. [CrossRef]
23. Prasad, M. Velocity-permeability relations within hydraulic units. *Geophysics* **2003**, *68*, 108–117. [CrossRef]
24. Mavko, G.; Mukerji, T.; Dvorkin, J. *The Rock Physics Handbook; Tools for Seismic Analysis in Porous Media*; Cambridge University Press: Cambridge, UK, 1998; Volume 1, 329p.
25. Mavko, G.; Mukerji, T. A rock physics strategy for quantifying uncertainty in common hydrocarbon indicators. *Geophysics* **1998**, *63*, 1997–2008. [CrossRef]
26. Dandekar, D.P. Pressure dependence of the elastic constants of calcite. *Phys. Rev. B* **1968**, *172*, 873–877. [CrossRef]
27. Voigt, W. *Lehrbuch der Kristallphysik: (Mit Ausschluss der Kristalloptik)*; BG Teubner: Berlin, Germany, 1910; Volume 34.
28. Bhimasenachar, J. Elastic constants of calcite and sodium nitrate. *Proc. Indian Acad. Sci. Sect. A* **1945**, *22*, 199. [CrossRef]
29. Peselnick, L.; Robie, R.A. Elastic constants of calcite. *J. Appl. Phys.* **1963**, *34*, 2494–2495. [CrossRef]
30. Gebrande, H. Rock forming minerals: Datasheet from Landolt-Börnstein-Group V Geophysics. In *Elastic Wave Velocities and Constants of Elasticity at Normal Conditions*; Angenheister, G., Ed.; Springer: Berlin/Heidelberg, Germany, 1982.
31. Fabricius, I.L.; Baechle, G.; Eberli, G.P.; Weger, R. Estimation of permeability of carbonate rocks from porosity and vP/vS data by applying Kozeny's equation. In *Challenges in Seismic Rock Physics: Summer Workshop, June 25–29, Beijing 2007*; RIPED, PetroChina, University of Houston & Colorado School of Mines: Beijing, China, 2007.
32. Kozeny, J. Uber Kapillare Leitung der Wasser im Boden. *Sitzungsberichte Wien. Akad. Wiss.* **1927**, *136*, 271–306.
33. Weger, R.J.; Eberli, G.P.; Massaferro, J.L.; Sun, Y.; Baechle, G.T. Theoretically Derived Pore Geometry in Carbonates Using the Extended Biot Theory. *Mar. Pet. Geol.* **2023**, *155*, 106359. [CrossRef]
34. Sun, Y.F. *Pore Structure Effects on Velocity-Porosity Relationship in Carbonates*; Technical Report EP2001-5092; Shell EPT: The Hague, The Netherlands, 2001; p. 19.
35. Dunham, R.J. *Classification of Carbonate Rocks According to Depositional Texture*; Memoir; American Association of Petroleum Geologists: Tulsa, OK, USA, 1962; pp. 108–121.
36. Choquette, P.W.; Pray, L.C. Geologic nomenclature and classification of porosity in sedimentary carbonates. *Am. Assoc. Pet. Geol. Bull.* **1970**, *54*, 207–244.
37. Birch, F. The velocity of compressional waves in rocks to 10 kilobars: 1. *J. Geophys. Res.* **1960**, *65*, 1083–1102. [CrossRef]
38. Baechle, G.T.; Eberli, G.P.; Weger, R.J.; Massaferro, J.L. Changes in dynamic shear moduli of carbonate rocks with fluid substitution. *Geophysics* **2009**, *74*, E135–E147. [CrossRef]
39. Berg, B.V.; Grammer, M.; Eberli, G.P.; Weger, R.J. Combining pore architecture and sonic velocity response to predict reservoir quality: An example from a mid-continent mississippian carbonate. In Proceedings of the Adapted from an Oral Presentation Given at AAPG Mid-Continent Section Meeting, Wichita, KS, USA, 12–15 October 2013.
40. Norbisrath, J.H.; Eberli, G.P.; Weger, R. Complex resistivity spectra and fractal pore geometries in relation to flow properties in carbonate rocks. In Proceedings of the AAPG Annual Convention and Exhibition, Denver, CO, USA, 3 June 2015.
41. Verwer, K.; Eberli, G.P.; Weger, R.J. Effect of pore structure on electrical resistivity in carbonates. *AAPG Bull.* **2011**, *95*, 175–190. [CrossRef]
42. Weger, R.J.; Giddens, E.; MacKenzie, G.; Eberli, G.P. Uniform Petrophysical Properties of Carbonate Contourite Drifts. In Proceedings of the 36th International Meeting of Sedimentology, Dubrovnik, Croatia, 12–16 June 2023; Vlahović, I., Matešić, D., Eds.; Croatian Geological Society: Dubrovnik, Croatia, 2023.

43. Weger, R.J. Quantitative Pore/Rock Type Parameters in Carbonates and Their Relationship to Velocity Deviations. Ph.D. Thesis, University of Miami, Coral Gables, FL, USA, 2006.
44. Mortensen, J.; Engstrøm, F.; Lind, I. The relation among porosity, permeability, and specific surface of chalk from the Gorm field, Danish North Sea. *SPE Reserv. Eval. Eng.* **1998**, *1*, 245–251. [CrossRef]
45. Sun, Y.F. *On the Foundations of the Dynamical Theory of Fractured Porous Media and the Gravity Variations Caused by Dilatancies*; Columbia University, UMI: Ann Arbor, MI, USA, 1994; p. 189.
46. Sun, Y.F.; Goldberg, D. Estimation of aspect-ratio changes with pressure from seismic velocities. In *Developments in Petrophysics*; Lowell, M.A., Harvey, P.A., Eds.; Geological Society, Special Publications: London, UK, 1997; pp. 131–139.
47. Sun, Y.F.; Massaferro, J.L.; Eberli, G.; Teng, Y.C. Quantifying the Effects of Pore Structure and Fluid Saturation on Acoustic Wave Velocity in Carbonates. In *Theoretical and Computational Acoustics*; World Scientific: Singapore, 2001; pp. 335–347.
48. Kleis, S.; Sanchez, L. Dependence of speed of sound on salinity and temperature in concentrated NaCl solutions. *Sol. Energy* **1990**, *45*, 201–206. [CrossRef]
49. Verwer, K.; Braaksma, H.; Kenter, J.A. Acoustic properties of carbonates: Effects of rock texture and implications for fluid substitution. *Geophysics* **2008**, *73*, B51–B65. [CrossRef]
50. Hillgärtner, H.; Dupraz, C.; Hug, W. Microbially induced cementation of carbonate sands: Are micritic meniscus cements good indicators of vadose diagenesis? *Sedimentology* **2001**, *48*, 117–131. [CrossRef]
51. Diaz, M.R.; Eberli, G.P.; Weger, R.J. Fast Rates of Microbially-Mediated Early Marine Cements. In Proceedings of the 36th International Meeting of Sedimentology, Dubrovnik, Croatia, 12–16 June 2023; Vlahović, I., Matešić, D., Eds.; Croatian Geological Society: Dubrovnik, Croatia, 2023.
52. Wyllie, M.R.J.; Gregory, A.R.; Gardner, L.W. Elastic wave velocities in heterogeneous and porous media. *Geophysics* **1956**, *21*, 41–70. [CrossRef]
53. Simmons, G. Single crystal elastic constants and calculated aggregate properties. *J. Grad. Res. Cent.* **1965**, *34*, 1.
54. Anderson, O.L.; Liebermann, R.C. *Sound Velocities in Rocks and Minerals*; VESIAC State-of-the-Art Report No. 7885-4-x; University of Michigan: Ann Arbor, MI, USA, 1966.
55. Schlumberger. *Log Interpretation Charts*; Publication SMP-7006; Schlumberger, Ltd.: Houston, TX, USA, 1984.
56. Humbert, P.; Plicque, F. Proprietes elastiques de carbonates rhombohedriques monocristallins: Calcite, magnesite, dolomite. *Comptes Rendus L'academie Sci. Paris* **1972**, *275*, 391–394.
57. Nur, A.; Simmons, G. The effect of viscosity of a fluid phase on velocity in low porosity rocks. *Earth Planet. Sci. Lett.* **1969**, *7*, 99–108. [CrossRef]
58. Chen, C.-C.; Lin, C.-C.; Liu, L.-G.; Sinogeikin, S.V.; Bass, J.D. Elasticity of single-crystal calcite and rhodochrosite by Brillouin spectroscopy. *Am. Mineral.* **2001**, *86*, 1525–1529. [CrossRef]
59. Dandekar, D.P. Variation in the elastic constants of calcite with temperature. *J. Appl. Phys.* **1968**, *39*, 3694–3699. [CrossRef]
60. Hearmon, R. The elastic constants of crystals and other anisotropic materials. *Landolt-Bornstein Tables* **1984**, *3*, 559.
61. Vo Thanh, D.; Lacam, A. Experimental study of the elasticity of single crystalline calcite under high pressure (the calcite I—Calcite II transition at 14.6 kbar). *Phys. Earth Planet. Inter.* **1984**, *34*, 195–203. [CrossRef]